Potent LILRB1 D1D2-containing antibodies inhibit RIFIN-mediated immune evasions

Yizhuo Wang[1,2,#], Hengfang Tang[1,#], Wanxue Wang[2,3], Ming Li[2], Chenchen Zhu[1,2], Han Dai[1], Hongxin Zhao[1,4,*], Bo Wu[2,*], Junfeng Wang[1,2,*]

[1]High Magnetic Field Laboratory, Key Laboratory of High Magnetic Field and Ion Beam Physical Biology, Hefei Institutes of Physical Science, Chinese Academy of Sciences, Hefei, Anhui 230031, China.

[2]University of Science and Technology of China, Hefei, Anhui 230026, China.

[3]Department of Anatomy, School of Basic Medical Sciences, Anhui Medical University, Hefei, China.

[4]Hefei China Science Longwood Biological Technology Co., Ltd. Hefei, Anhui 230088, China.

[#] Those authors contributed equally.

*Corresponding authors. Email: zhx@hmfl.ac.cn (Hongxin Zhao), wubo@hmfl.ac.cn (Bo Wu), junfeng@hmfl.ac.cn (Junfeng Wang).

Abstract

Variant surface antigens of *Plasmodium falciparum*, including RIFIN, play a key role in malaria pathogenesis and promote immune evasion by binding to immunoinhibitory receptors such as LILRB1. Recently, receptor-containing antibodies have been identified in malaria-exposed individuals and reveal a novel antibody mechanism for inhibiting immune evasions in *Plasmodium falciparum*. Previous studies have identified several LAIR1- and LILRB1 D3D4-containing antibodies. However, no antibodies containing LILRB1-D1D2 have been identified, although some RIFINs interact with LILRB1-D1D2 to mimic the binding mode of β2-microglobulin, a major histocompatibility complex (MHC) class I molecules. In this study, we propose an in vitro strategy for generating receptor-containing antibodies through structure-based affinity maturation. Using this strategy, we successfully generated a LILRB1 D1D2-containing antibody, D1D2.v-IgG, which effectively blocked the specific binding of RIFIN#1 (from PF3D7_1254800) to LILRB1-D1D2 domains. Furthermore, we developed NK-biAb, a D1D2.v-IgG-based bispecific antibody targeting RIFIN#1 and NKG2D receptors. Both antibodies showed promising results in enhancing NK cell-mediated cytotoxicity against RIFIN#1-expressing K562 cells, with NK-biAb being more efficacious. The present strategy can be generalized for the development of antibodies against Plasmodium-host interactions, thus contributing to the advancement of malaria treatments and vaccines.

Keywords: *Plasmodium falciparum*, immune evasion, RIFIN, receptor-containing antibody

45 **Introduction**

46 Malaria is one of the most deadly infectious diseases affecting human health,
47 causing nearly half a million deaths each year. The disease is caused by *Plasmodium*
48 infections, of which *Plasmodium falciparum* (*P. falciparum*) is the deadliest
49 species[1,2]. The emergence and spread of drug-resistant parasites threaten global malaria
50 control and raise the demand for novel malaria treatments and vaccines[3-5].

51 The life cycle of *P. falciparum* is complex, comprising multiple developmental
52 stages from the mosquito vector to the human host. Of these, the blood stage is
53 responsible for the clinical symptoms of malaria[6,7]. During this stage, *P. falciparum*
54 invades and replicates in erythrocytes and also expresses a number of variable surface
55 antigens on infected erythrocytes (IEs). Blood-stage parasites are the main target of
56 acquired immunity. However, *P. falciparum* employs multiple strategies to evade
57 immune responses by interacting with host receptors through variable surface antigens,
58 which is thought to contribute to the slow development of naturally acquired immunity
59 against malaria. PfEMP1 and RIFIN are two of the three major multigene familiy
60 proteins expressed on the surface of IEs. PfEMP1 proteins were found to interact with
61 various human endothelial receptors and mediate the adhesion of the IEs to blood
62 vessels and tissues surfaces, thereby helping *P. falciparum* to evade splenic clearance.
63 RIFINs are the largest family of variable surface antigens of *P. falciparum*[7,8]. Some
64 RIFINs have been shown to mediate immunosuppression by binding to and activating
65 inhibitory immune receptors on myeloid and lymphoid cells , such as leukocyte-
66 associated immunoglobulin-like receptor 1 (LAIR1) and leukocyte immunoglobulin-
67 like receptor B1 (LILRB1)[9-12] (Fig. 1a). Theoretically, blocking those surface antigen-
68 receptor interactions, thereby preventing the immune escape of *Plasmodium*, maybe a
69 promising strategy for development of effective malaria treatments and vaccines[13,14].
70 Notably, LAIR1- and LILRB1-containing antibodies have recently been found in

71 malaria-infected individuals, suggesting that the human immune system employs this

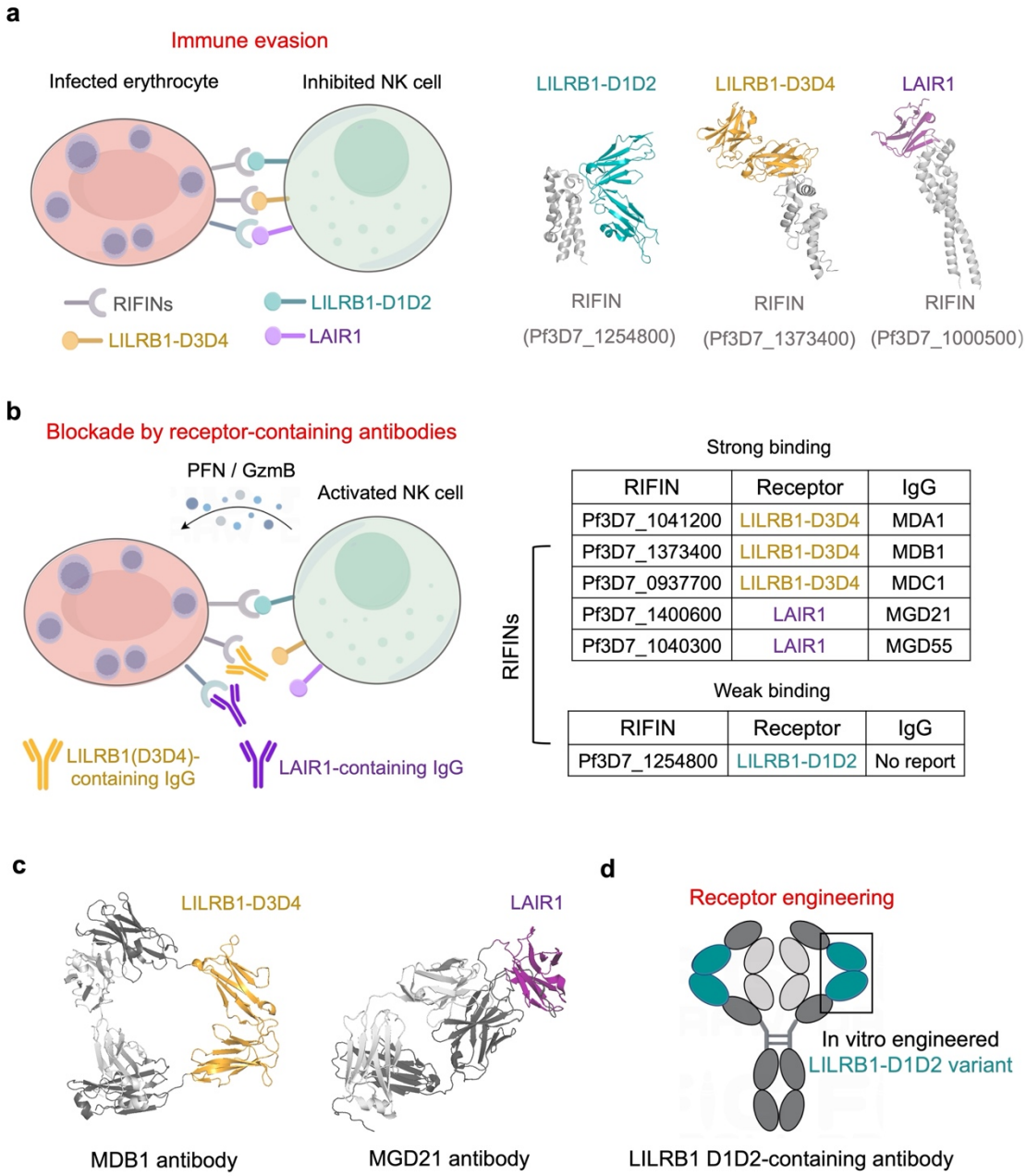

72

73 **Figure 1. Immune evasion of *P.falciparum* and design of novel receptor-containing antibody**

74 (**a**) Mechanisms of immune evasion of *P. falciparum* and structures of RIFIN and immunoinhibitory

75 receptors**.** Different RIFIN isoforms bind to their corresponding receptor domains and transduce

76 immunosuppressive signals (PDB: 6ZDX, 7KFK and 7F9N). (**b**) Receptor-containing antibodies in

77 inhibiting immune evasion of *P. falciparum* and identification of LILRB1- and LAIR1-containing

78 antibodies. All reported LILRB1-containing antibodies only have LILRB1-D3D4 domains and no

79 antibodies that contain LILRB1-D1D2 domains were found. (**c**) Two representative receptor-

containing antibody. The left one is LILRB1 D3D4-containing antibody MDB1 (PDB:7KHF) and the right one is LAIR1-containing antibody MGD21 (PDB: 7JZ4). (**d**) Strategy for generating high-affinity LILRB1 D1D2-containing antibodies. The affinity-matured LILRB1-D1D2 variant was generated through structure-based affinity maturation in vitro and then the LILRB1-D1D2 variant was grafted into the framework of MDB1 by replacing LILRB1-D3D4 domains.

strategy to counteract immune evasions of malaria parasites[15-17] (Fig. 1b). The LAIR1-containing antibodies reveal specific mutations in the LAIR1 insert, resulting in high affinity toward RIFINs[16]. Unlike the LAIR1-containing antibodies, the LILRB1-containing antibodies reveal no mutation in LILRB1 inserts and all LILRB1 inserts are LILRB1-D3D4 domains or just LILRB1-D3 domain within the variable-constant (VH-CH1) elbow region[15] (Fig. 1c). Some RIFINs bind to LILRB1-D1D2, mimicking the binding pattern between LILRB1-D1D2 and MHC class I. However, no antibodies containing the LILRB1-D1D2 structural domain have been identified, probably due to the low affinity of RIFINs for LILRB1-D1D2. In addition, the formation of receptor-containing antibodies in vivo is time-consuming, especially during the in vivo affinity maturation process, and the maturation site of receptor-containing antibodies is uncontrollable.

Here, we propose a strategy for designing novel receptor-containing antibodies. Our strategy is to obtain a high-affinity receptor fragment variant by structure-based affinity maturation in vitro [18-20] , and then graft the affinity-matured receptor fragment variants into the framework of the human anti-malaria natural antibody MDB1 by replacing the LILRB1-D3D4 structural domain in MDB1 (Figure 1d). Using this strategy, a novel LILRB1 D1D2-containing antibody, D1D2.v-IgG, was successfully generated. D1D2.v-IgG binds to RIFIN with 110-fold higher affinity than LILRB. Biochemical and cellular assays demonstrated that D1D2.v-IgG blocked the RIFIN#1-LILRB1 interaction, and significantly enganced the NK cell-mediated cytotoxicity against RIFIN#1-expressing K562 cells. In addition, based on the D1D2.v-IgG, a bi-

108 specific antibody NK-biAb was engineered by incorporating the natural killer group 2
109 D (NKG2D) receptor-specific scFv KYK2.0[21-23] at its C-terminus, mimicking CAR-
110 NK therapy[24,25]. Notably, NK-biAb exhibits an enhanced capacity to augment NK cell-
111 mediated cytotoxicity compared to D1D2.v-IgG. Our work provides a novel approach
112 to the design of antibodies targeting the interaction between surface antigens of
113 Plasmodium variants and host receptors, which may contribute to the development of
114 malaria therapeutics and vaccines.

115 **Results**

116 **Structure-guided engineering of a high affinity LILRB1 D1D2 variant**

117 RIFIN#1 binds to the extracellular domain (ECD) of LILRB1 through its variable
118 region with a moderate affinity (K_d =570 ± 130 nM). LILRB1-ECD comprises four
119 immunoglobulin-like domains (D1-D4), and its complex structure with RIFIN#1
120 suggests that the interaction is mediated by the D1D2 domain[9]. In order to obtain a
121 high-affinity variant capable of competitively antagonizing LILRB1-RIFIN#1
122 interaction, we performed structure-guided directed evolution of the LILRB1-D1D2
123 domain by yeast surface display. A library of LILRB1 D1D2 mutations was designed
124 using the structure of the LILRB1-RIFIN#1 complex as a guide. As shown in Figure
125 2a, ten LILRB1 D1D2 residues (K42, E68, G97, A98, Y99, I100, Q125, V126, F128,
126 E184) interfacing with RIFIN#1 were altered based on the structural information by
127 randomized PCR. The resulting D1D2 mutant library contained $2x10^7$ transformants.
128 The library was then displayed on the yeast surface, stained with biotinylated RIFIN ,
129 and screened to isolate high-affinity binders (Fig. 2b and Fig. S1). In total, eight round
130 of sorting were performed (Fig. S2). Three rounds of sorting with decreasing
131 concentrations of biotinylated RIFIN tetramers (2 μM, 1 μM and 0.3 μM) (Fig. S3) and
132 three rounds of sorting with decreasing concentrations of biotinylated RIFIN monomers
133 (0.3 μM, 0.1μM and 0.02 μM) (Fig. S4) were performed for binder enrichment. For
134 kinetic sorting, enriched library was screened using 0.02 μM biotinylated RIFIN
135 monomers in the presence of approximately a 50-fold excess unlabeled competition

RIFIN, with a duration of 2 h and 4 h respectively (Fig. S5). After completion of all eight rounds of sorting, yeast cells were transplanted to obtain individual clones. DNA sequencing results indicate that a single D1D2 mutant clone (named D1D2.v) dominates this enrichment process, and this consensus variant contains a total of nine mutations: K42M, G97S, A98T, Y99F, I100T, Q125E, V126I, F128Q, E184H (Fig. 2c and Fig. S6).

To gain insight into the mechanisms of D1D2.v affinity enhancement, we obtained a structural model of D1D2.v binding to RIFIN#1 using SWISS-MODEL (Fig. 2d). Comparative analysis with the crystal structure of the LILRB1-RIFIN#1 complex show that D1D2.v binds to RIFIN#1 in essentially the same manner as its wild-type counterpart; however, some differences are observed at the binding interface. As shown in Figure 2d, the Q125E mutation establishes a new salt bridge with R233 on RIFIN#1. In addition, the G97S, A98T, and I100T mutations appears to enhance the strength of their H-bonds with RIFIN#1 based on analysis of the H-bond distance.

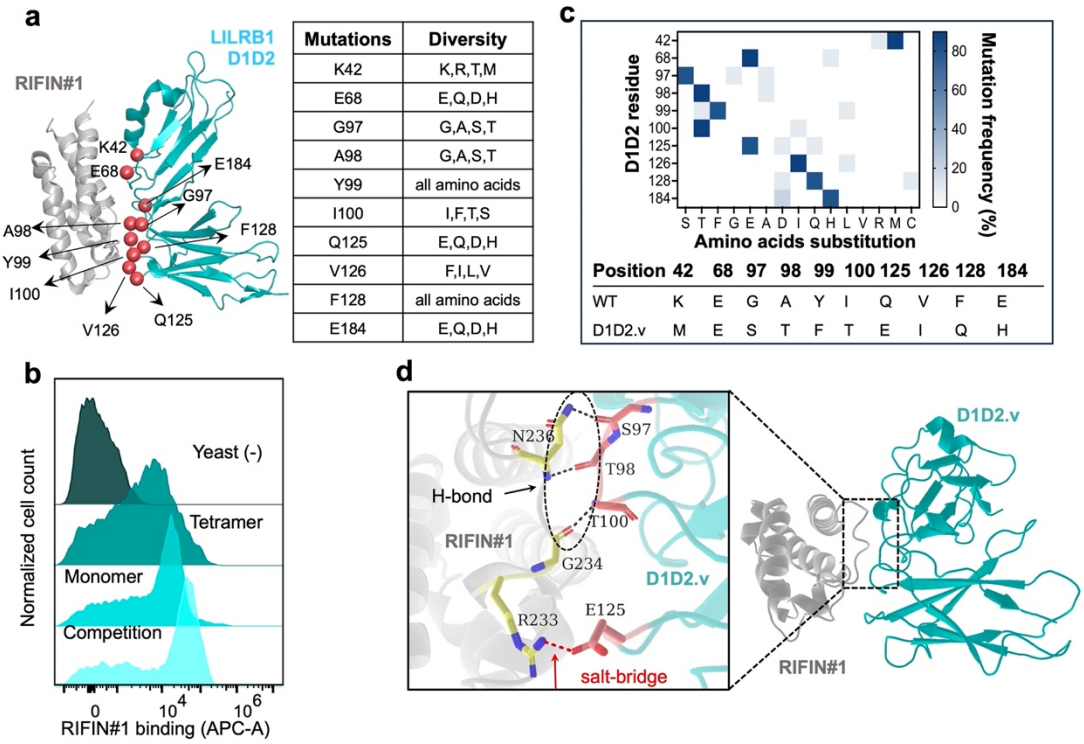

Figure 2. Yeast display and affinity maturation of D1D2 domain

152 (**a**) (Left) LILRB1 models based on LILRB1-RIFIN#1 complex structure (PDB:6ZDX), where
153 RIFIN#1 is in orange color, LILRB1-D1D2 is in cyan color, and the randomized positions are
154 depicted by red balls; (Right) Table of random positions of the LILRB1-D1D2 interface library with
155 possible amino acid variants. (**b**) Flow cytometry results for the yeast stained with biotinylated
156 RIFIN#1 in tetramer, monomer and competition selection strategy. (**c**) Mutation frequencies (Above)
157 and consensus D1D2.v sequence (Below). (**d**) Structural modeling and interface analysis. The
158 sequences of D1D2.v and RIFIN#1 were imported into the SWISS-MODEL server for initial model
159 generation based on the coordinates of PDB code**.** The G97S, A98T, I100T and Q125E mutations
160 in D1D2.v increases H-bonding strength targeting RIFIN#1, while a salt-bridge forms between
161 E125 on D1D2.v and R233 on RIFIN#1.
162
163
164 **Design and biochemical characterization of a D1D2.v-containing antibody that**
165 **antagonizes RIFIN#1-LILRB1 interaction.**
166 Recently, several natural LILRB1-containing monoclonal antibodies were
167 identified in malaria-infected individuals, such as MDB1, in which the LILRB1 D3D4
168 structural domain was inserted into its variable-conatant(VH-CH1) elbow region[15,16].
169 We then replaced the LILRB1-D3D4 insertion domain in MDB1 with D1D2.v to
170 generate a D1D2-containing antibody, named D1D2.v-IgG (Fig. 3a). To express as the
171 secreted protein, the codon-optimized antibody sequence was genetically linked to a N-
172 terminal Trp2 signal peptide sequence within a pTT5 expression vector. The
173 recombinant antibody was transiently expressed in Expi293F cells and purified from
174 culture supernatant by protein A affinity chromatography. The purity was confirmed by
175 SDS-PAGE analysis under both non-reducing and reducing conditions. To evaluate the
176 RIFIN#1-binding activity of this recombinant antibody, we generated the Fab fragment
177 by enzymatically removing the Fc tag and detected its binding with RIFIN#1 by size-
178 exclusion chromatography (SEC) assay. The results showed that Fab bound strongly to
179 RIFIN#1, forming a tight complex (Figure 3b). Next, we quantified the binding affinity

of D1D2.v-IgG to RIFIN#1 using a protein-based ELISA assay with purified LILRB1 ECD as a control. As shown in Fig. 3c, the dissociation constant (K_d) for LILRB1 ECD binding to RIFIN#1 was approximately 650 nM, which is consistent with the previously reported affinity determined using surface plasmon resonance (SPR). In contrast, the affinity of D1D2.v-IgG binding to RIFIN#1 was significantly higher, with a K_d of 6 nM, a 110-fold increase (Fig. 3c). To assess the ability of D1D2.v-IgG to antagonize the binding of LILRB1 to RIFIN#1, we performed a competitive ELISA assay. The results showed that D1D2.v-IgG effectively inhibited the binding of LILRB1 to RIFIN#1 in a dose-dependent manner with a half-maximal inhibitory concentration (IC_{50}) of 20 nM (Fig. 3d).

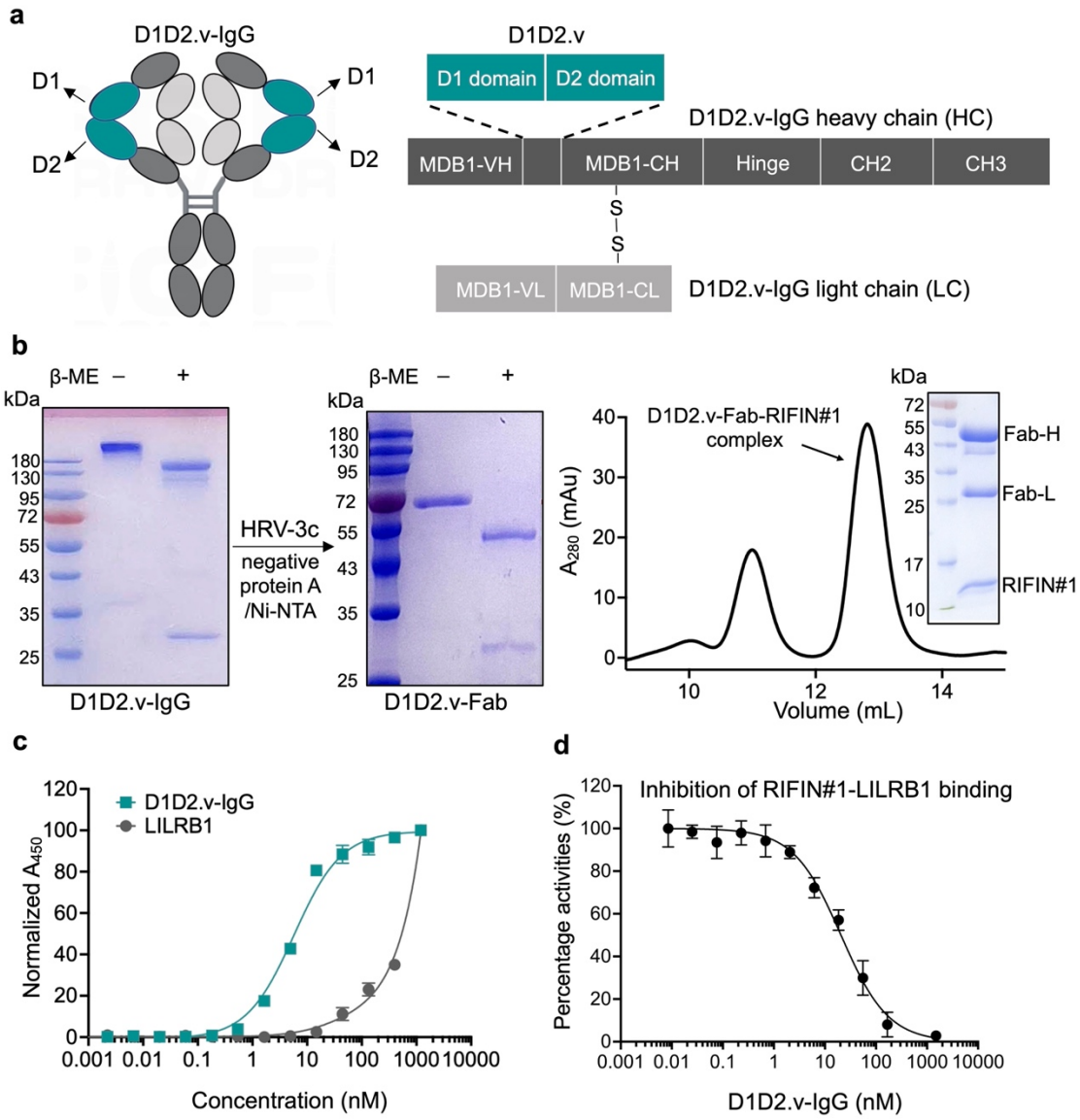

191 **Fig.3: Molecular design and biochemical characterization of the D1D2.v-IgG**

192 **(a)** Molecular structure and cDNA frame of LILRB1 D1D2-containing IgG. The inserted LILRB1-
193 D1 domain is colored in dark blue and LILRB1-D2 domain is colored in light blue, which are located
194 between heavy variable chain (VH) and heavy constant chain (CH). The antibody heavy chain and
195 Fc domain are depicted in dark grey and the light chain is depicted in light grey. **(b)** Purification
196 and functional validation of the antigen binding fragment (Fab) of D1D2.v-IgG. SDS-PAGE (Left)
197 show the purity and molecular weight of D1D2.v-IgG before protease digestion. SDS-PAGE (Right)
198 show the purity and molecular weight of D1D2.v-Fab. Size-exclusion chromatography (SEC)
199 chromatograms show the homogeneous Fab-RIFIN complex have a UV_{280} absorbance at around 13
200 mL. **(c)** Titration curves of wild-type LILRB1 (ECD) (dark green) and D1D2.v-IgG (red) binding
201 to RIFIN in ELISA assay. Data are mean ± SD. **(d)** The representative competition binding curve
202 using wild type LILRB1 (ECD) show D1D2.v-IgG antagonizes the RIFIN-LILRB1 (ECD)
203 interaction effectively. Data represent mean ± SD of three technical replicates.

204

205

206 **D1D2.v-IgG significantly enhances NK92 cytolytic activity against RIFIN#1-**
207 **expressing K562 cells in vitro**

208 Given that RIFIN#1 binding to LILRB1 inhibits NK cell responses, we
209 subsequently investigated whether D1D2.v-IgG could enhance NK cell-mediated
210 cytotoxicity by blocking the interaction between LILRB1 and RIFIN#1. To assess this,
211 we performed NK92 cell cytotoxicity assays on K562 cells stably transfected with full
212 length RIFIN#1 (Fig. S7). Flow cytometry verified the expression level of LILRB1 on
213 NK92 cells (Fig. 4a). The RIFIN#1-expressing K562 cells were co-cultured with NK92
214 cells at two different effector to target (E:T) ratios of 2.5 and 12.5 in the presence or
215 absence of D1D2.v-IgG. Flow cytometry analysis confirmed the specific binding of
216 purified D1D2.v-IgG to the RIFIN#1-expresssing K562 cells (Fig. 4b). The
217 cytotoxicity against K562 cells expressing RIFIN#1 was 5.8% in the absence of
218 D1D2.v-IgG when the E:T ratio was 2.5, and increased significantly to 13.8% when

D1D2.v-IgG at a concentration of 100 nM was added. Similarly, when the E:T ratio was 12.5, the cell killing efficiency was 35% in the absence of D1D2.v-IgG, but increased significantly to 61% when D1D2.v-IgG at a concentration of 100 nM was added (Fig. 4c). In addition, we observed that D1D2.v-IgG significantly increased the secretion of perforin and granzyme B from NK92 cells (Fig. 3d-e). These findings clearly indicate that D1D2.v-IgG can effectively stimulate NK-cell cytotoxicity against RIFIN#1-expressing K562 cells.

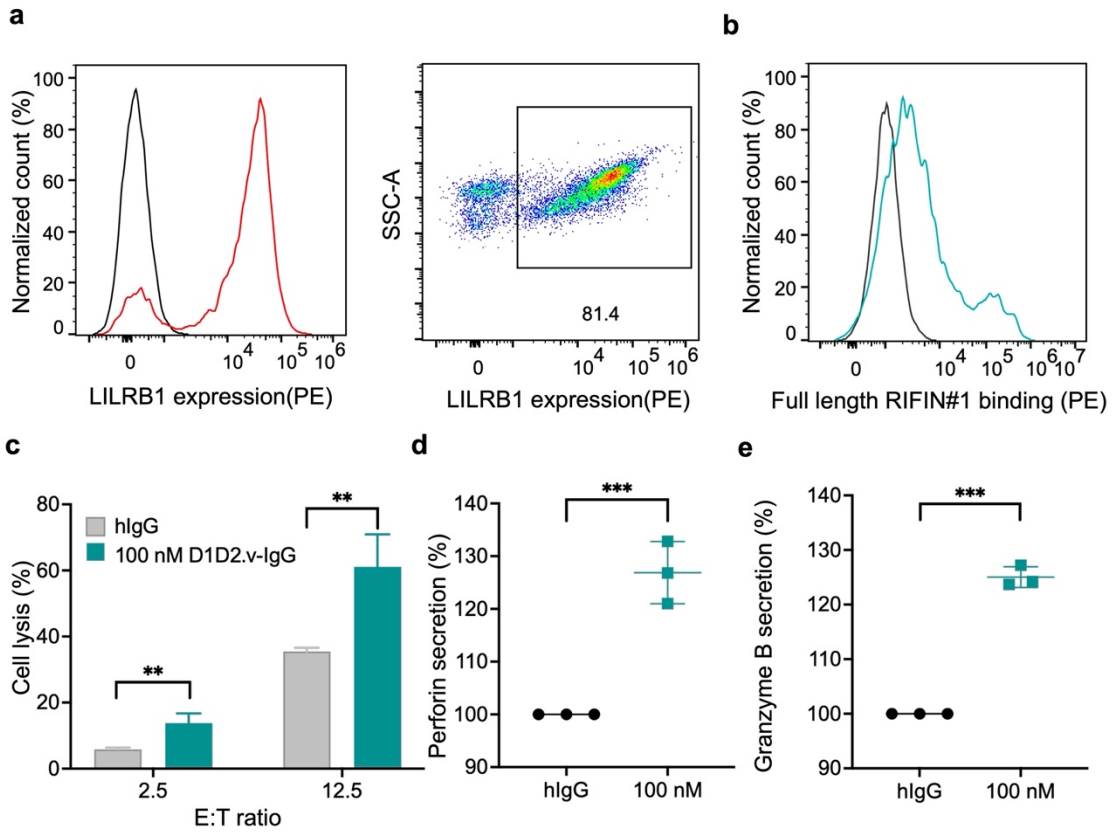

Fig.4: D1D2.v-IgG enhanced NK cell cytotoxicity against RIFIN-expressing K562 cell

(a) Detection of the LILRB1 on NK92 cells by flow cytometry. The red curve shows the binding of LILRB1 antibody to LILRB1 on NK92 cells, while the blue curve informs the control sample of NK92 cells. **(b)** Detection of the purified D1D2.v-IgG bound to RIFIN#1-expressing K562 cells by flow cytometry. The red curve shows the binding of D1D2.v-IgG to full-length RIFIN#1 on stably-transfected K562 cells, while the cyan curve informs the blank sample of K562 cells. **(c)** The results for the NK92 cytotoxicity in the presence or absence of D1D2.v-IgG. RIFIN#1-expressing K562 cells were cocultured with NK92 cells and incubated with 100 nM control human IgG (hIgG) (Grey,

n = 3) or 100 nM D1D2.v-IgG (Yellow, n = 3). (**d,e)** Detections of the perforin (e) and granzyme B (f) releases in the presence or absence of D1D2.v-IgG. RIFIN#1-expressing K562 cells were cocultured with NK92 cells (E: T ratio = 1: 1) and incubated with 100 nM control hIgG (Grey, n = 3) or 100 nM D1D2.v-IgG (Orange, n = 3). After the incubation for 24h, the perforin and granzyme B levels were determined by ELISA. Statistical test was t test and statistical significance was analyzed between D1D2.v-IgG and hIgG. *P<0.05; **P<0.01; ***P<0.001; ****P<0.0001.

Generation of a bispecific antibody targeting RIFIN#1 and NKG2D

Next, we developed a bispecific antibody that recruits NK cells to RIFIN#1-expressing cells using the D1D2.v-IgG as a basis. The redirection of NK cells requires a highly specific and high-affinity 'compass' (Fig. 5a). To fulfill this requirement, we chosen an engineered scFv called KYK2.0, which exhibits a nanomolar affinity towards NKG2D expressed on all types of NK cells. By fusing the scFv form of KYK2.0 to the C terminal of the Fc fragment of D1D2.v-IgG via a flexible GS linker, we generated a bispecific antibody (bsAb), named NK-biAb (Fig. 5b). The resulting bsAb was then transiently expressed and purified from Expi293F cell culture supernatants by affinity chromatography. Integrity and purity of NK-biAb were analyzed by SDS-PAGE under reducing and non-reducing conditions (Fig. S8a). As exprected, this purified bispecific antibody demonstrated the ability to bind to both NK cells and RIFIN#1-expressing K562 cells in flow cytometry analysis (Fig. S8b-c).

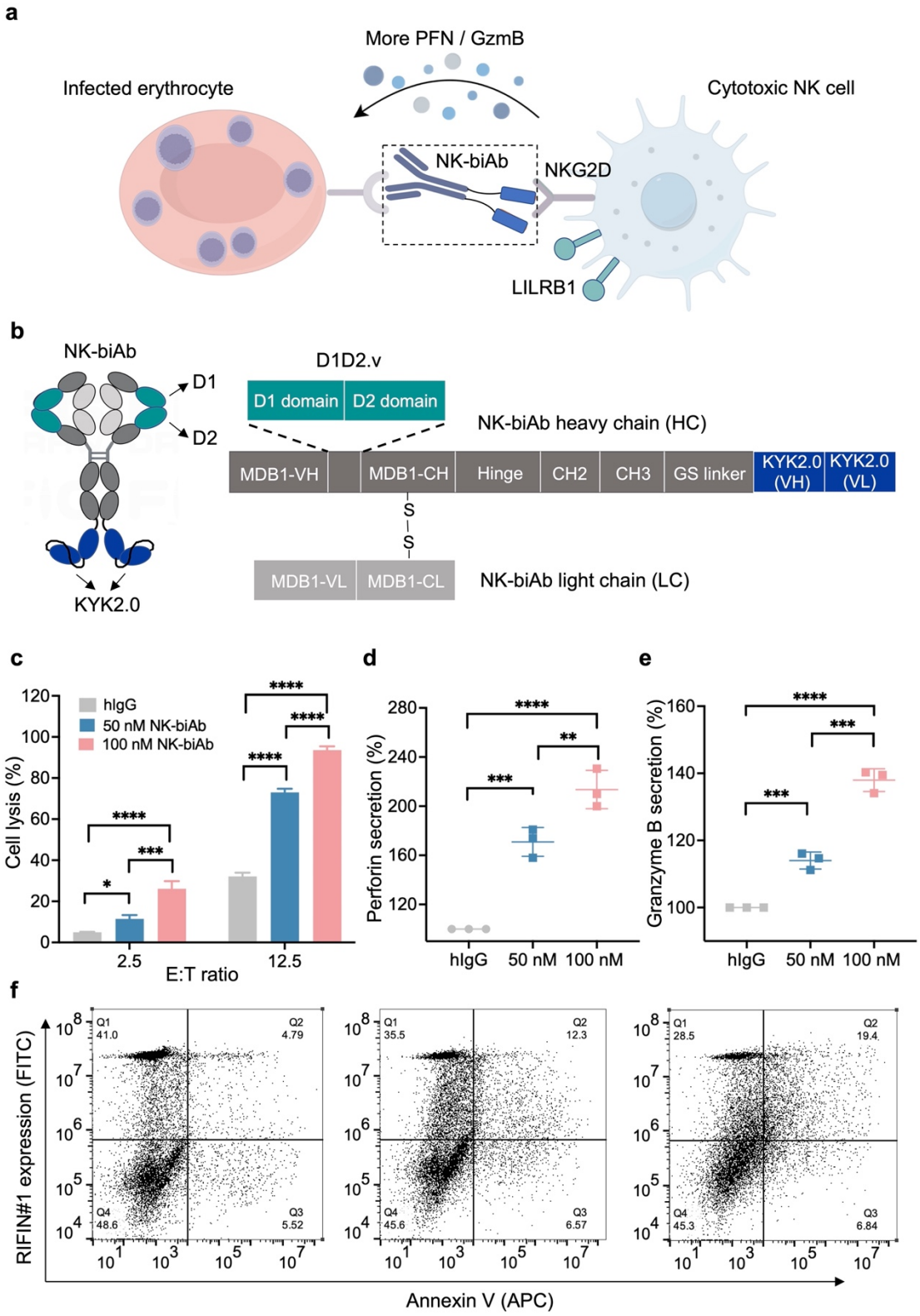

Fig.5: Design and characterization of NK-biAb

(a) Schematic of NK cell redirections by NK-biAb. Scfv form of KYK2.0 (scfv-KYK2.0), an NKG2D activating antibody was fused to C terminus of D1D2.v-IgG. When recognizing and blocking immune escape response of *P. falciparum* via D1D2.v-Fab domains, scfv-KYK2.0 domain

262 can also bind to NKG2D receptors, redirect NK cells to *P. falciparum* and trigger NK cell activities.
263 scFv-KYK2.0 is colored in light orange and NKG2D receptor is depicted as a light blue dart.
264 **(b)** cDNA frame of NK-biAb. cDNA of D1D2.v-IgG part is the same as previously described. The
265 heavy variable chain (VH) and light variable chain (VL) of KYK2.0 depicted in orange are fused to
266 C terminus of D1D2.v-IgG by a GS linker. (**c)** NK92 cytotoxicity assay in the presence of NK-biAb.
267 RIFIN#1-expressing K562 cells were cocultured with NK92 cells and incubated with 100 nM
268 control human IgG (hIgG) or 50 nM NK-biAb (Cyan, n =3) and 100 nM NK-biAb (Red, n =3).
269 Statistical tests were two-way ANOVA and statistical significance was analyzed between NK-biAb
270 and hIgG. **(d,e)** Detections of the perforin (d) and granzyme B (e) releases in the presence or absence
271 of NK-biAb. RIFIN#1-expressing K562 cells were cocultured with NK92 cells (E: T ratio = 1: 1)
272 and incubated with 100 nM control hIgG (Grey, n = 3), 50 nM NK-biAb (Cyan, n =3) and 100 nM
273 NK-biAb (Red, n = 3). After the incubation for 24h, the perforin and granzyme B levels were
274 determined by ELISA. Statistical tests were one-way ANOVA and statistical significance was
275 analyzed between NK-biAb and hIgG. **(f)** Flow detection results for the coculture of NK92 and
276 RIFIN#1-expressing K562 for 24 h at E: T = 1: 1 in the presence of 100 nM hIgG (Left), 50 nM
277 NK-biAb (Middle) and 100 nM NK-biAb (Right), showing the RIFIN#1-expressing K562 cells
278 killed by NK92 cells. The data in the second quadrant stands for the lysed RIFIN#1-expressing
279 K562 cells. *P<0.05; **P<0.01; ***P<0.001; ****P<0.0001.
280
281
282 **NK-biAb exhibits an enhanced ability to trigger NK92 cytotoxicity against**
283 **RIFIN#1-expressing K562 cells.**
284 Finally, we evaluated the effect of NK-biAb on NK cell cytotoxicity against
285 RIFIN#1-expressing K562 cells. As shown in figure, the ability of this bispecific
286 antibody to trigger NK cytotoxicity was significantly enhanced compared to the
287 monospecific antibody D1D2.v-IgG. When treatment with NK-biAb at a concentration
288 of 100 nM, there was a remarkable enhancement in cytotoxic efficiency from 13.8% to
289 26.1% and from 61%-93.6%, at E/T ratios of 2.5 and 12.5 respectively, compared to

290 treatment with D1D2.v-IgG under the same conditions (Fig. 5c). Compared with
291 D1D2.v-IgG treatment, NK92 cells secreted more perforin and granzyme B in the
292 presence of 50 nM and 100 nM NK-biAb (Fig. 5d-5e). Flow cytometry results also
293 verified that NK-biAb can potently stimulate NK-cell cytotoxicity against RIFIN#1-
294 expressing K562 cells (Fig. 5f).
295
296
297 **Discussion**
298 Upon infection, *P. falciparum* utilizes variant surface antigens to engage with
299 receptors on the human host, thereby facilitating immune evasion and ensuring their
300 survival in the host[7,8]. Recent studies have identified several receptor-containing
301 antibodies in malaria-exposed individuals that block surface antigen-receptor
302 interactions. Functional studies have shown that these antibodies hold potential as
303 therapeutic agents and for incorporation into malaria vaccine design[15-17]. For instance,
304 MGD21 antibody has been shown to promote NK cell-dependent cleavage of IEs and
305 to inhibit the growth of *P. falciparum*[17]. However, reported receptor-containing
306 antibodies only have either LAIR1 domain or LILRB1-D3D4 domains, and no
307 antibodies containing LILRB1-D1D2 domains have been discovered. The RIFIN
308 family is divided into different species, some of which interact with LILRB1-D1D2
309 domains rather than LILRB1-D3D4 domain or LAIR1 to transduce immunoinhibitory
310 signals. Therefore, the use of LILRB1 D1D2-containing antibodies for the treatment of
311 malaria is of great importance.
312 In this study, we propose an in vitro strategy for designing novel receptor-
313 containing antibodies. Our approach utilizes structure-guided affinity maturation to
314 obtain receptor fragment variants with enhanced binding capacity, while using the
315 framework of a human natural antibody against malaria as a template for antibody
316 generation[15]. Due to the weak affinity between RIFIN and LILRB1-D1D2, no relevant
317 D1D2-containing antibody has been reported. We used this strategy to artificially create

318 high-affinity D1D2-containing antibodies, filling a gap in this field. As an illustrative
319 example, we successfully prepared D1D2.v-IgG antibody, which has 110-fold higher
320 affinity towards RIFIN1# than LILRB1 and can effectively block the interaction
321 between RIFIN1# and LILRB1. Cellular experiments demonstrated that D1D2.v-IgG
322 significantly enhanced NK cell-mediated cytotoxicity against K562 cells expressing
323 RIFIN#1. In addition, on the basis of D1D2.v-IgG, we developed a bispecific antibody
324 targeting both RIFIN#1 and the NKG2D receptor, which showed enhanced ability to
325 trigger NK cell-mediated cytotoxicity compared to D1D2.v-IgG. Bispecific antibodies
326 have been shown to be a promising avenue for immunotherapeutic interventions in a
327 variety of malignancies[21,22,24,26]. Our data emphasize the potential application of these
328 agents in combating malaria.
329 In conclusion, our study provides a strategy for the design of receptor-containing
330 antibodies, offering potential applications in the development of malaria therapeutics
331 and vaccines. The increasing availability of resolved structures of Plasmodium surface
332 antigens binding to host receptors[9,11,15,17] will facilitates the development of
333 corresponding antibodies using our strategy.
334
335 **Materials and Methods**
336 **Antigen purifications**
337 The variable region of RIFIN#1 (PF3D7_1254800, 165-274 aa) with an N-
338 terminal 6×His tag was cloned into a pET28a vector. The recombinant vector was
339 transformed into E.coli BL21 (gold), and the cells were induced with 1 mM IPTG at a
340 OD_{600} of 0.7. Protein was expressed as inclusion bodies and denatured in a guanidine
341 buffer (6 M Guanidine hydrochloride, 20 mM Tris pH 8.0, and 300 mM NaCl) for 4 h.
342 The inclusion bodies were then purified by Ni-NTA affinity chromatography and eluted
343 by the guanidine buffer containing additional 500 mM imidazole. The denatured
344 inclusion bodied were retrieved by dialyzing against a buffer (20 mM Tris pH 8.0, 300
345 mM NaCl) and resolubilized in the guanidine buffer. Refolding was performed by the

346 quick dilution of inclusion bodies into a buffer (1 M L-arginine, 20 mM Tris pH 8.5,
347 100 mM NaH_2PO_4, 2 mM ethylenediaminetetraacetic acid, 0.1 mM
348 phenylmethylsulfonyl fluoride, 3 mM reduced glutathione and 0.3 mM oxidized
349 glutathione) until a final protein concentration of 0.1 mg/mL-0.2 mg/mL. The refold
350 RIFIN#1 was further polished on a Superdex 75 Increase column in a PBS (pH 7.2)
351 buffer. The ECD of human LILRB1 gene with a C-terminus His tag was cloned into a
352 pTT5 vector, and the vector was then PEI-transfected into Expi293F cells (Procell,
353 China). After a post-transfection for 96 h, the supernatant was collected and the protein
354 was purified with a Ni-NTA affinity chromatography. The purified LILRB1-ECD was
355 further exchanged into PBS (pH 7.2) buffer on a Superdex 200 Increase column.
356 For biotinylation, the RIFIN#1 and LILRB1-ECD proteins were cultured with
357 NHS-pEG12-biotin in a PBS buffer (pH 7.2). The culture reactions were quenched with
358 a Tris buffer after 8 h incubation. The free NHS-pEG12-biotin reagents were splitted
359 from the biotin-labeled proteins by a size-exclusion chromatography.
360
361 **EBY100 vector construction and LILRB1-D1D2 wild type display**
362 To avoid weird display stuff, pYD1 vector was reconstructed by fusing Agar 1/2
363 domain to the C-terminus of displayed targets. Meanwhile, the detection tags of pYD1
364 vector were replaced by a N-terminal FLAG, a C-terminal V5-tag and a C-terminal His
365 tag. D1D2 wild type was co-electroporated with a precut reconstructed pYD1, while
366 yeast cells were induced with SGCAA. The signals of RIFIN#1 binding to the displayed
367 D1D2 wild type were detected by FCM.
368
369 **Constructing the library of D1D2 variants**
370 Based on the crystal structure of RIFIN#1-LILRB1 complex, a site-directed
371 library was generated by the several rounds of overlapping PCR reactions for
372 randomizing the binding residues of LILRB1-D1D2. The randomizing primers are as
373 shown in Supplementary Table 1.The overlapping PCR reactions were conducted under

374 20 cycles. The external primers for the amplification of LILRB1-D1D2 library on a
375 large scale introduce a 70 bp homologous sequence to pYD1 vector. The LILRB1-
376 D1D2 library were co-transformed into EBY100 with a precut pYD1 vector at a
377 library/vector ratio of 3: 1. Yeast transformants were recovered in a YPD/Sorbitol broth
378 and amplified in SDCAA, resulting in a library containing 2×10^7 transformants.
379
380 **MACS selections of the naive library**
381 Transformed yeast were induced in SGCAA medium at 20°C for 48 h. For the 1st
382 round selection, 4×10^8 cells referred to as 20× library size were pellet and washed with
383 a PBE buffer (PBS pH 7.2 supplemented with 0.5% BSA). Firstly, the cells were
384 resuspended in 2 mL of the PBE buffer containing 2 μM biotinylated RIFIN that had
385 been pre-coated with Streptavidin-Alexa Fluor 647 (Invitrogen, USA), followed by an
386 incubation at 4°C for 2 h. Secondly, the stained cells were pelleted by centrifugation
387 (3500 g, 5 min) , washed twice with 2 mL PBE, and resuspended in PBE containing
388 paramagnetic anti-Alexa Fluor 647 microbeads (Miltenyi Biotech, German). Thirdly, a
389 magnetically-labeled yeast cells were enriched on LS MACS column (Miltenyi Biotech,
390 German), and the enriched yeast cells were eluted with 5-10 mL PBE. Finally, the
391 selection outputs were pellet and amplified in SDCAA for next round selection. Five
392 additional selections were performed by successively decreasing concentrations of
393 biotinylated RIFIN#1 from 1 μM to 0.02 μM. In each round selection, the yeast cells
394 were first labeled with SAV-Alexa Fluor 647 after incubating with biotinylated
395 RIFIN#1 for 2 h and washed once with PBE, then coated with 100 μL of anti-Alexa
396 Fluor 647 microbeads for 30 min and washed once, and finally separated by LS MACS
397 column.
398
399 **MACS competition selections**
400 The MACS tetramer/monomer selection outputs were further performed
401 competition selections to get ultrahigh affinity variants. The induced tetramer/monomer

402 selection outputs were cultured with 0.02 μM biotinylated RIFIN#1 at 4°C for 2 h. Then
403 the cells were pellet, washed once with PBE and competed with 1 μM unlabeled
404 RIFIN#1 for 2 h. After the competition process, the cells were stained with
405 Streptavidin-Alexa Fluor 647 and coated with anti-Alexa Fluor 647 microbeads. MACS
406 sorting was also performed using LS column. By now, the 1st round competition was
407 finished, and the competition outputs were amplified and induced for next round
408 competition selection. In the 2nd round competition selection, the competing time of
409 unlabeled RIFIN was increased to 4 h, and the final selection outputs were titrated on
410 SDCAA plates for plasmid extraction and sequencing.
411
412 **Preparation of D1D2.v-IgG**
413 D1D2.v were inserted between MDB1-VH and MDB1-CH, and cloned into pTT5
414 vector as IgG4 forms. MDB1 light chain was also cloned to pTT5 vector. The DNAs
415 of MDB1 light chains and D1D2.v-IgG heavy chains were co-transfected into
416 Expi293F cells using PEI transfection reagents. After the transfection for 96 h, the
417 culture supernatant was separated by centrifugation (4000 rpm, 10 min) and purified
418 with protein A resin. The purified D1D2.v-IgG was further polished on a Superdex 200
419 Increase column in a PBS (pH 7.4) buffer.
420
421 **Characterization of D1D2.v-IgG**
422 Protein-based ELISA assays were performed to determine the affinity of D1D2.v-
423 IgG to RIFIN#1 in comparison to that of LILRB1-ECD. First, RIFIN#1 (5 μg/mL) was
424 immobilized on 96-well ELISA plates and incubated with D1D2.v-IgG of different
425 concentrations. Then, the plates were washed with PBST for 3 times and cultured with
426 the anti-human IgG-HRP at 1: 5000 dilution. Finally, the wells were washed with PBST,
427 developed with TMB for 15 min, and quenched with 2 M HCl. The absorbance at 450
428 nm was determined by a microplate reader.

429 For the protein-competition ELISA assay, RIFIN#1 (5 μg/mL) was immobilized
430 on 96-well ELISA plates, and cocultured with D1D2.v-IgG of different concentrations
431 and a competing biotinylated LILRB1 (ECD) of 1-1.5× K_d concentration, where K_d is
432 the dissociation constant. Then the plates were washed with PBST for 3 times and
433 cultured with HRP-conjugated streptavidin at 1: 2000 dilution. The absorbance at 450
434 nm was recorded by a microplate reader.
435
436 **Purifying Fab fragment of D1D2.v-IgG and its functional validation**
437 D1D2.v-IgG was digested by His-tagged HRV-3c protease overnight and
438 subjected to a negative protein A and Ni-NTA column purification. The 5-fold excess
439 of refold RIFIN#1 were co-cultured with the Fab fragment of D1D2.v-IgG and the
440 resulting complex was further polished on a Superdex 200 Increase column. The ratio
441 of RIFIN#1 binding to the Fab fragment of D1D2.v-IgG was assessed by SDS-PAGE.
442
443 **Preparation of NK-biAb and its functional validation**
444 scFv-KYK2.0 was fused to the C-terminus of D1D2.v-IgG heavy chain to generate
445 NK-biAb (M_r = 260 kDa). The DNAs of MDB1 light chains and NK-biAb heavy chains
446 were co-transfected into Expi293F cells using PEI transfection reagents. After the
447 transfection for 96 h, the culture supernatant was collected by centrifugation (4000 rpm,
448 10 min) and purified on a protein A column. The purified protein was further polished
449 on a Superdex 200 Increase column in a PBS (pH 7.4) buffer. To validate the functions
450 of NK-biAb to attach NK92 cells and bind NKG2D, the NK92 cells pre-stimulated with
451 IL-2 were cultured with NK-biAb at 37°C for 2 h, and stained with anti-human IgG-PE
452 for the detection of surface NKG2D.
453
454 **Stable RIFIN#1-expressing K562 cell line production**
455 K562 cells (Procell, China) were cultured at 37°C in DMEM with 10% FBS and
456 5% CO_2. The cDNA of RIFIN#1 with its natural signal peptide was cloned into pLVX-

457 ZsGreen plasmid. Lentivirus were produced by HEK-293T (Procell, China) for
458 infecting K562 cells. The infected K562 cells were enriched by the selection using 1
459 μg/mL puromycin, to obtain the stable RIFIN#1-expressing K562 cell line.
460
461 **Evaluation of NK cell cytotoxicity**
462 The RIFIN#1-expressing K562 cells were incubated at 37°C for 1 h with D1D2.v-
463 IgG or NK-biAb. The NK92 cells in the same volume as RIFIN#1-expressing K562
464 cells were then cocultured for 4 h at 37°C and 5% CO_2 with the incubated RIFIN#1-
465 expressing K562 cells at the E: T ratios of 2.5: 1 and 12.5: 1. The final mixtures contain
466 either 100 nM D1D2.v-IgG or 50 nM/100 nM NK-biAb. The killing efficiency (E) was
467 calculated from the absorbance (A) of CCK8 at 450 nm: $E\% = [1-(A_S-A_{EC})/A_{TC}]\times 100\%$,
468 where A_S is for the mixture of effector and target cells, and A_{EC} and A_{TC} are, respectively,
469 for effector cells and target cells.
470
471 **Cytokine measurement and FCM detection**
472 10^5 NK92 cells were cocultured for 24 h with 10^5 RIFIN#1-expressing K562 cells
473 in a 96-well plate in the presence of either 100 nM D1D2.v-IgG or 50 nM/100 nM NK-
474 biAb. Perforin and granzyme B release were detected from the supernatants of the
475 cocultured mixture by protein-based ELISA assay kits (Beyotime, China). The mixtures
476 of NK92 and K562-RIFIN#1 cells were stained for 1 h at 4°C (controlled by ice) with
477 Annexin V-APC in 100 μL PBS containing 0.5% BSA. The stained cells were detected
478 by flow cytometry, with the data analyzed by Flowjo software.
479
480
481
482 **Reference**
483 1. World Malaria Report 2023 [M]. World Health Organization (2023).

484 2. Burton, D. R. Antibodies, viruses and vaccines. *Nature Reviews Immunology* **2**, 706-
485 713 (2002).
486 3. Haldar, K., Bhattacharjee, S. & Safeukui, I. Drug resistance in *Plasmodium*. *Nature*
487 *Reviews Microbiology* **16**, 156-170 (2018).
488 4. Burton, D. R. What Are the Most Powerful Immunogen Design Vaccine Strategies?
489 Reverse Vaccinology 2.0 Shows Great Promise. *Cold Spring Harb Perspect Biol*
490 **9**(2017).
491 5. Wells, T. & Donini, C. Monoclonal Antibodies for Malaria. *New England Journal of*
492 *Medicine* **387**, 462-465 (2022).
493 6. Nilsson, S. K., Childs, L. M., Buckee, C. & Marti, M. Targeting Human Transmission
494 Biology for Malaria Elimination. *PLOS Pathogens* **11**, e1004871(2015).
495 7. Sakoguchi, A. & Arase, H. Mechanisms for Host Immune Evasion Mediated by
496 *Plasmodium falciparum*-Infected Erythrocyte Surface Antigens. *Frontiers in*
497 *Immunology* **13** (2022).
498 8. Chan, J. A., Fowkes, F. J. & Beeson, J. G. Surface antigens of *Plasmodium*
499 *falciparum*-infected erythrocytes as immune targets and malaria vaccine candidates.
500 *Cell Mol Life Sci* **71**, 3633-3657(2014).
501 9. Harrison, T. E. *et al.* Structural basis for RIFIN-mediated activation of LILRB1 in
502 malaria. *Nature* **587**, 309-312 (2020).
503 10. Saito, F. *et al.* Immune evasion of *Plasmodium falciparum* by RIFIN via inhibitory
504 receptors. *Nature* **552**, 101-105 (2017).
505 11. Xie, Y. *et al.* Structural basis of malarial parasite RIFIN-mediated immune escape
506 against LAIR1. *Cell Rep* **36**, 109600 (2021).
507 12. Willcox, B. E., Thomas, L. M. & Bjorkman, P. J. Crystal structure of HLA-A2
508 bound to LIR-1, a host and viral major histocompatibility complex receptor. *Nature*
509 *Immunology* **4**, 913-919 (2003).

510 13. Wahl, I. & Wardemann, H. How to induce protective humoral immunity against
511 *Plasmodium falciparum* circumsporozoite protein. *Journal of Experimental Medicine*
512 **219** (2022).
513 14. Cockburn, I. A. & Seder, R. A. Malaria prevention: from immunological concepts
514 to effective vaccines and protective antibodies. *Nature Immunology* **19**, 1199-1211,
515 doi:10.1038/s41590-018-0228-6 (2018).
516 15. Chen, Y. *et al.* Structural basis of malaria RIFIN binding by LILRB1-containing
517 antibodies. *Nature* **592**, 639-643 (2021).
518 16. Tan, J. *et al.* A LAIR1 insertion generates broadly reactive antibodies against
519 malaria variant antigens. *Nature* **529**, 105-109 (2016).
520 17. Xu, K. *et al.* Structural basis of LAIR1 targeting by polymorphic *Plasmodium*
521 RIFINs. *Nature Communications* **12**, 4226 (2021).
522 18. Chao, G. *et al.* Isolating and engineering human antibodies using yeast surface
523 display. *Nature Protocols* **1**, 755-768(2006).
524 19. Weiskopf, K. *et al.* Engineered SIRPα variants as immunotherapeutic adjuvants to
525 anticancer antibodies. *Science* **341**, 88-91(2013).
526 20. Gonzalez-Perez, D. *et al.* Affinity-matured DLL4 ligands as broad-spectrum
527 modulators of Notch signaling. *Nature Chemical Biology* **19**, 9-17(2023).
528 21. Kwong, K. Y., Baskar, S., Zhang, H., Mackall, C. L. & Rader, C. Generation,
529 affinity maturation, and characterization of a human anti-human NKG2D monoclonal
530 antibody with dual antagonistic and agonistic activity. *J Mol Biol* **384**, 1143-
531 1156(2008).
532 22. Zhang, C. *et al.* Bispecific antibody-mediated redirection of NKG2D-CAR natural
533 killer cells facilitates dual targeting and enhances antitumor activity. *J Immunother*
534 *Cancer* **9** (2021).
535 23. Zhao, C. *et al.* A new approach to produce IgG (4)-like bispecific antibodies. *Sci*
536 *Rep* **11**, 18630 (2021).

24. Wolf, N. K., Kissiov, D. U. & Raulet, D. H. Roles of natural killer cells in immunity to cancer, and applications to immunotherapy. *Nature Reviews Immunology* **23**, 90-105 (2023).

25. Albinger, N., Hartmann, J. & Ullrich, E. Current status and perspective of CAR-T and CAR-NK cell therapy trials in Germany. *Gene Therapy* **28**, 513-527 (2021).

26. Leaver-Fay, A. *et al.* Computationally Designed Bispecific Antibodies using Negative State Repertoires. *Structure* **24**, 641-651 (2016).

Acknowledgements: Funding was provided by the National Key R&D Program of China (Grant No. 2023YFA1607500), the National Natural Science Foundation of China (Grant No. 32371362), and the Anhui Major Basic Research Projects (Grant No. 2023z04020016).

Author contributions: Y.W and H.T contributed equally to this work. Y.W initiated the project, performed the library construction and selections, prepared antigen samples and performed biochemical assays. H.T performed the FCM detections and conducted the stable cell line production, cytotoxicity assays and ELISA assays. W.W performed the antibody purifications and functional validations. L.M helped to prepare biotinylated sample preparations. C.Z helped to perform biochemical assays and FCM detections. Y.W. and B.W analyzed the data, interpreted the results. J.W, H.D and B.W prepared the manuscript. J.W., B.W and H.Z supervised the project. All authors read and edited the manuscript.

Competing interests: The authors declare no competing interests.

Data and materials availability: All data and materials are available within the paper and its supplementary materials. Extra data are available from the corresponding author (J. Wang) upon reasonable request.

List of Supplementary Materials

Fig S1 to S8 for multiple supplementary figures

Table S1 for supplementary table